Research Article | Vol. 33, No. 21 / 20 Oct 2025 / Optics Express 44474
Optics EXPRESS

Cryoless MIR spectroscopy via pump wavelength scanning using PPLN ridge waveguide upconversion

ABHISHEK RAI,[1] LUDOVIC GROSSARD,[1,*] TRISTAN CHABROL,[1] FRANÇOIS REYNAUD,[1] MATHIEU CHAUVET,[2] FLORENT BASSIGNOT,[3] AND RODOLPHE KRAWCZYK[4]

[1]*Univ. Limoges, CNRS, XLIM, UMR 7252, 123 Avenue Albert Thomas, Limoges 87000, France*
[2]*Université Marie et Louis Pasteur, CNRS, Institut FEMTO-ST, F-25000 Besançon, France*
[3]*Femto-Engineering, 15B Avenue des Montboucons, 25000 Besançon, France*
[4]*Thales Alenia Space, Observation Exploration & Navigation (Retired), 5 Allée des Gabians BP 99, Cannes La Bocca Cedex 06156, France*
[*]*ludovic.grossard@unilim.fr*

Abstract: This article presents what we believe to be a novel room-temperature mid-wave Infrared spectroscopy (MWIR) technique utilizing upconversion in a 2 cm-long PPLN ridge waveguide. Addressing limitations of costly, cryo-dependent FTIR, our "non-linear spectrometer" samples MWIR spectra by sweeping a low-power, continuous wave monochromatic pump laser, enabling detection with sensitive silicon detectors. Experimental validation with a channelled spectrum demonstrated accurate thermal source spectral modulation recovery, showing a 3% relative error. This robust approach offers a promising pathway for miniaturized, practical MIR spectroscopic tools.

1. Introduction

Mid-Infrared (MIR) spectroscopy has emerged as an established tool in diverse technical and scientific fields including biological and pharmaceutical sciences [1,2], astronomy [3], free space communications [4], environmental monitoring and gas sensing [5]. The MIR spectral range is particularly interesting for the detection of many gaseous molecules. These photons have energies too low to excite an atomic electronic transition, but correspond to vibrational and rotational energy transitions in many gaseous molecules. What's more, fundamental transitions in the MIR have much more pronounced absorption lines than their harmonics usually detected in the visible and near-infrared [6]. In particular, the medium wave infrared (MWIR) spectral range, which extends from 3 to 5 µm, enables the detection of many trace gases (e.g. CO_2, CO, CH_4, dimethyl sulfide) and compound molecules (HCHO, C_2H_5OH, and more generally hydrocarbons that exhibit absorption around 3.4 µm due to the C–H bond).

One of the commonly used standard technique is Fourier transform infrared spectroscopy (FTIR) [7,8]. This technique relies on interferometric systems (usually Michelson or Mach-Zehnder) which require a moving mirror to reconstruct the spectrum from the interferogram measurement. Despite its widespread use, FTIR faces several challenges. Firstly, they are expensive and complex to implement, which limits their field of application. Secondly, they require excellent mechanical stability when the mirror is moved. The presence of mechanical vibrations can greatly impair system accuracy. Finally, FTIR spectroscopy suffers from the limited performance of the detectors available in MIR, in terms of low efficiency and noise. The InSb and mercury cadmium telluride detectors traditionally used exhibit significant dark noise

#575043 https://doi.org/10.1364/OE.575043
Journal © 2025 Received 30 Jul 2025; revised 28 Aug 2025; accepted 14 Sep 2025; published 13 Oct 2025

Optics EXPRESS

due to thermal noise, and Planck radiation from the detector itself and its surroundings. It is therefore necessary to cool these sensors using heavy and complex cryogenic systems [9].

Upconversion is an alternative method to traditional techniques for detecting MWIR light. This indirect method overcomes the limitations of direct MWIR detection and spectroscopy techniques. The MWIR signal is transferred into the near-infrared (NIR) and visible range through an inherently noiseless [10] second order non-linear process. This technique offers several key advantages over direct MWIR detection. It is particularly sensitive and low-noise, since it allows the use of mature and readily available Silicon-based detectors [11], including in the photon-counting regime [12]. Thanks to the change in wavelength of the signal to be analyzed, it is possible to work at room temperature without the need for a cryogenic system. The main drawback of the upconversion technique is the conversion spectral bandwidth limited by the quasi-phase-matching condition of the non-linear process [13].

Numerous MWIR radiation detection studies based on upconversion have been carried out in recent years. Most of them use a bulk periodically poled lithium niobate (PPLN) as a non-linear medium, renowned for its high non-linear coefficient. Spectral analysis is then carried out after frequency conversion using an NIR spectrometer. However, the short interaction length between the waves in the non-linear medium requires it to be placed intracavity in order to work with pump powers of several watts or tens of watts [14]. Several strategies have been explored to increase the converted MWIR spectral bandwidth, such as chirped poling structures [15], fanout structures [16,17], or by exploiting the inflection point of the collinear quasi-phase-matching curve [18], at the expense of conversion efficiency.

In this article, we present a new technique for detecting MWIR radiation using upconversion, based on the use of a 2 cm-long PPLN ridge waveguide. The long interaction length between the fields and the good spatial overlap of the modes in the waveguide enable single-pass operation with a continuous wave (CW), monochromatic tunable laser of just a few tens of mW power [19]. The aim is to convert the smallest possible MWIR spectral band into the NIR range, to sample the spectrum of the source to be analyzed, and to detect the converted flux in the photon-counting regime. The source spectrum is then reconstructed by sweeping the pump laser wavelength, resulting in a sweep of the MWIR-converted spectral band due to quasi-phase-matching conditions in the non-linear waveguide. The so-called "non-linear spectrometer" system requires no spectral analysis of the converted signal at the end of the acquisition chain, since spectral selectivity is achieved by the non-linear process itself. The resolution of this system is then given by the spectral acceptance width of the non-linear waveguide, i.e. the spectral width of the MWIR sample converted by the monochromatic pump laser line.

To validate our detection technique, we generated a channelled spectrum using an interferometer introduced between a thermal source and the non-linear spectrometer to periodically modulate the spectrum of light emitted by the source. We were able to recover the modulation period after upconversion by continuously scanning the wavelength of the pump laser. The modulation period obtained experimentally has a relative error of around 3%, proving the credibility of this technique.

The article is organized as follows. Section 2 presents the theoretical fundamentals of the non-linear spectrometer. In Section 3, we describe the experimental set-up used to measure the modulation period of the thermal source spectrum. Section 4 shows experimental results and discussion, followed by a conclusion.

2. Basic concept of non-linear spectroscopy

The non-linear process of sum frequency generation (SFG) enables signal radiation in the MIR range to be shifted into the NIR domain by means of pump laser radiation, which energizes the MIR photons. For a monochromatic pump laser beam, the interaction between a pump photon with a frequency of ν_p and a signal photon with a frequency of ν_s results in the creation of a

Optics EXPRESS

converted photon with a frequency of ν_c. This process is governed by the principle of energy conservation:

$$\nu_p + \nu_s = \nu_c \tag{1}$$

For a pump power P_p, and under the assumption of a weak conversion regime and no pump depletion during the non-linear process, the conversion efficiency is quantified by the ratio of the number of converted photons, denoted by N_c, to the number of input signal photons, denoted by N_s. The conversion efficiency is thus expressed as follows:

$$\eta(\nu_s, \nu_p) = \frac{N_c}{N_s} = \eta_{\text{nor}} \cdot P_p \cdot L^2 \cdot \text{sinc}^2\left(\frac{\Delta k L}{2}\right)$$

where L is the interaction length (in the case of a non-linear waveguide, it corresponds to the waveguide length), and Δk is the phase mismatch of the non-linear process [13].

The utilization of a PPLN waveguide allows one to benefit from a very high non-linear coefficient and easy-to-design quasi-phase-matching conditions by periodic inversion of the ferroelectric domains of the material. The phase mismatch is then given by:

$$\Delta k = 2\pi\left(\frac{n_s\nu_s}{c} + \frac{n_p\nu_p}{c} - \frac{n_c\nu_c}{c} + \frac{1}{\Lambda}\right)$$

where n_s, n_p and n_c are the effective indices of the propagating modes inside the waveguide for the signal, pump and converted wave respectively. Λ is the domain inversion period of the PPLN waveguide.

For a given pump frequency ν_p, $\eta(\nu_s)$ defines the spectral acceptance curve of the non-linear waveguide. The shape of the spectral acceptance depends only on the phase mismatch, while its amplitude is related to the interaction length and the normalized conversion efficiency defined by (in $\text{W}^{-1}\text{m}^{-2}$):

$$\eta_{\text{nor}} = \frac{1}{A_{\text{eff}}} \cdot \frac{8\pi^2 d_{\text{eff}}^2 \nu_s \nu_c}{n_s n_p n_c c^3 \epsilon_0}$$

where d_{eff} is the effective non-linear coefficient. Assuming that the three interacting waves in the PPLN ridge waveguide all propagate in the fundamental mode (field mode radius w at $1/e$), A_{eff} is the effective area of the waveguide and is equal to $9\pi w^2/8$ and ϵ_0 is the vacuum permittivity.

If we consider the full width at half maximum $\Delta\nu_s$ of the spectral acceptance curve, the non-linear process powered by a monochromatic pump beam converts a spectral sample of $\Delta\nu_s$ width in the MIR domain to a spectral sample of $\Delta\nu_c$ width in the NIR domain such that $\Delta\nu_c = \Delta\nu_s$. Thus, the SFG process results in a shift by a quantity ν_p of the MIR spectral sample towards higher frequencies. The central frequency of the MIR spectral sample is directly related to the pump frequency through the quasi-phase-matching condition.

To retrieve the MIR spectrum of the source, we propose shifting the light emitted by this source from the MIR domain to the NIR domain using SFG, by scanning with the pump frequency. The number of measured photons per second in the NIR domain for this spectral sample as a function of the pump frequency ν_p is given by:

$$N_c(\nu_p) = \int B(\nu_s) \cdot \eta(\nu_s, \nu_p)\, d\nu_s \tag{2}$$

where $B(\nu_s)$ is the broadband MIR source power spectral density (PSD). If $\eta(\nu_s, \nu_p)$ is perfectly known, $B(\nu_s)$ can be reconstructed by inverting Eq. (2). In practical terms, this can be done using a matrix approach, discretizing the signal and pump frequencies involved in the non-linear

Optics EXPRESS

conversion:

$$N_c(\nu_p^i) = \sum_j B(\nu_s^j) \cdot \eta(\nu_s^j, \nu_p^i)\, \delta\nu_s \tag{3}$$

where $\delta\nu_s = \nu_s^{j+1} - \nu_s^j$ is the frequency difference between two consecutive signal frequency values. Let N_i (resp. N_j) be the number of samples for pump (resp. signal) frequencies

Equation (3) can then be expressed as a matrix product:

$$[N_c] = [B] \times [\eta]$$

Here, $[B]$ is a row vector representing the PSD of the MIR source. $[\eta]$ is the spectral conversion matrix, and is generally a rectangular matrix with N_j rows and N_i columns. Each column of $[\eta]$ corresponds to the spectral acceptance curve associated with the pump frequency ν_p^i, and gives the conversion efficiency as a function of the signal frequency ν_s^j.

Figure 1 shows the calculated spectral conversion matrix of a broadband MIR signal from 3.1 µm to 3.7 µm when the monochromatic pump wave scans from 1050 nm to 1080 nm. The parameters utilized for the simulation are given in the figure caption, and correspond to the experimental configuration that is described in the next section. When the quasi-phase-matching condition is met, the conversion quantum efficiency is near 5% for a pump power equal to 20 mW within the waveguide. As the wavelength of the pump increases, the spectral acceptance is shifted towards shorter signal wavelengths, while its full width at half maximum (FWHM) displays a slight decrease due to the quasi-phase-matching condition.

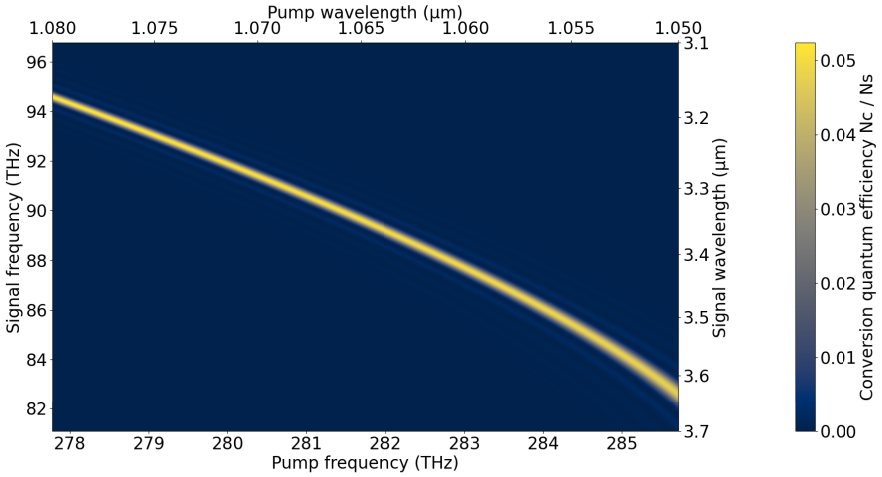

Fig. 1. Simulated Spectral Conversion Matrix as a function of the signal wavelength, ranging from 3.1 µm to 3.7 µm when the monochromatic pump wave scans from 1050 nm to 1080 nm. The simulation parameters are as follows: $A_{\text{eff}} = 31.8\ \mu\text{m}^2$, $L = 2$ cm, $d_{\text{eff}} = 15.26$ pm/V, $P_p = 20$ mW. The effective indices of the fundamental modes n_s, n_p and n_c are calculated using COMSOL for a waveguide cross-section with dimensions 8×8.6 µm. The poling period of the PPLN waveguide is $\Lambda = 19.6$ µm and its temperature is $T = 20°\text{C}$.

The MIR source PSD array denoted by $[B]$ can be subsequently retrieved from the measured converted photon counts array $[N_c]$, and the spectral conversion matrix $[\eta]$ using several techniques. First we can use the inverse of the $[\eta]$ matrix through a straightforward matrix product $[B] = [N_c] \times [\eta]^{-1}$ In order to calculate the inverse of the matrix of η (which is generally a rectangular matrix), we rely on Moore – Penrose pseudoinverse theorem [20] which states that inverse matrix can be calculated even if determinant of the matrix is zero and the matrix is not

Optics EXPRESS

square. Other methods are possible, such as Bayesian deconvolution or the use of neural networks or deep learning algorithms. The reconstruction of the original MIR spectrum is beyond the scope of this paper and will be addressed in a future study.

3. Experimental setup and general description

The experimental setup is illustrated in Fig. 2. The thermal source is constituted by a metallic wire driven by a 2 A current. The apparent temperature of the source was measured at 740 °C using a thermal camera. A set of two convergent CaF_2 lenses injects the MIR radiation emitted by the source into a ZBLAN fluoride glass (ZFG) single-mode fiber. This fiber is used to carry the radiation to the subsequent stage of the setup, while ensuring spatial filtering of the MIR radiation such that only the fundamental mode of the fiber is guided. A germanium filter (3 – 12 µm transmission) placed after the CaF_2 lenses eliminates all NIR radiation emitted by the source itself, which, in the absence of this filter, would otherwise result in the pollution of the radiation converted within the non-linear waveguide. At the output of the ZFG fiber, the MIR beam is collimated by an off axis parabola (OAP) and injected into a Michelson interferometer. One of the two mirrors of the interferometer has been shifted by $\delta x = 90$ µm to spectrally modulate the thermal source spectrum. The PSD of the MIR radiation at the output of the Michelson interferometer writes:

$$\mathrm{PSD}_{\mathrm{MIR}}(\nu_s) = \mathrm{PSD}^0_{\mathrm{MIR}}(\nu_s) \cdot \left[1 + \cos\left(2\pi \cdot \frac{2\delta x}{c} \cdot \nu_s\right)\right] \tag{4}$$

where $\mathrm{PSD}^0_{\mathrm{MIR}}$ is the spectral power density of the MIR field at the input of the interferometer. The spectral modulation periodicity of the resulting channeled spectrum is then given by $\Delta\nu = c/(2\delta x) = 1.67 \pm 0.15$ THz. The uncertainty on $\Delta\nu$ is due to the 10 µm resolution of the translation stage used to position the mirror. At the output of the interferometer, the two MIR beams are perfectly superimposed to avoid any spatial interference fringes. A spatially single-mode, vertically polarized pump beam is generated by a CW monochromatic laser diode (model TOPTICA DLC CTL 1050). The pump wave (laser linewidth lower than 100 pm) is

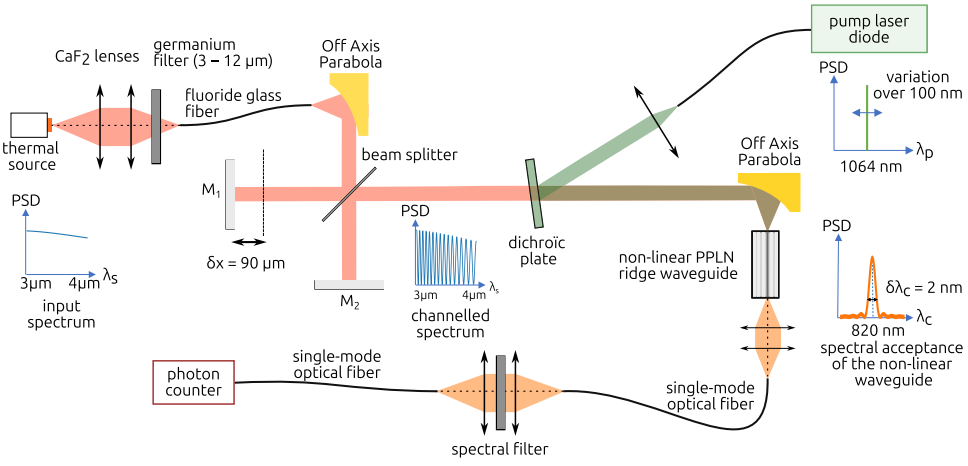

Fig. 2. Experimental setup. The spectrum of the MIR thermal source is modulated thanks to a Michelson interferometer. The MIR radiation is transposed to the NIR domain in the PPLN waveguide thanks to an upconversion process powered by a CW, monochromatic tunable pump laser. Converted photons are then filtered to remove any pump residue, and detected using a photon-counter. PSD: power spectral density.

Optics EXPRESS

continuously adjustable from 1010 nm to 1100 nm. The maximum output power for this laser is approximately 100 mW at 1055 nm. The pump beam and the MIR signal are then mixed by a Zn-Se dichroic plate, and then injected into the non-linear ridge waveguide using a second OAP. This ensures an optimal injection of the two fields at the same time without any chromatic effect. The waveguide is 2 cm long and its estimated average cross-section is equal to 8.6×8.0 μm^2. The poling period is equal to 19.6 μm to achieve a converted field near 810 nm for a pump beam around 1064 nm. The PPLN waveguide is maintained at 20 °C with a Peltier cooler associated with a Proportional–Integral–Derivative servo control system developed in the lab. Temperature fluctuations are in the order of 5×10^{-3} °C. At the output of the waveguide, the converted light is collected and injected into a single-mode polarization-maintaining (PM) fiber. A spectral filtering stage that utilizes three band-pass filters centered at 820 nm (Semrock FF01-820/12-25) enables the elimination of pump residues. The converted flux is then detected by a silicon avalanche photodiode (Si-APD) operating in the photon counting regime.

4. Experiments and results

Initially, the background noise of the experimental setup was characterized. It can be attributed to two primary sources:

- The electronic noise of the photon counter, which was measured at approximately 100 counts per second.
- The phenomenon of spontaneous parametric down conversion (SPDC). This noise is generated exclusively by the pump laser. A pump photon at 1064 nm spontaneously generates a signal photon around 3.4 μm, as well as the corresponding idler around 1550 nm (which plays no particular role here). This parasitic signal photon can then be converted into the NIR domain around 820 nm through the SFG process within the non-linear waveguide. The generation of noise photons through SPDC is significantly enhanced by PPLN fabrication errors, particularly random duty-cycle errors in the quasi-phase-matching grating [21] and evolves quadratically with pump power [22].

The noise level was recorded by blocking the signal beam from the thermal source and measuring the noise counts while the pump wavelength was scanned over the wavelength range from 1058 nm to 1080 nm. We have limited the pump scan over this range so that photons converted in the NIR range fall within the bandwidth of the spectral filters placed just before the photon counter. The evolution of the noise background as a function of pump wavelength is shown in Fig. 3. This noise undergoes a monotonic evolution, starting at 20,000 counts per second for a pump wavelength of 1058 nm, and decreasing to 11,000 counts per second at 1080 nm. The curve has been smoothed using a Savitzky-Golay filter [23], and will be subtracted later from all subsequent recordings.

Secondly, we determined the conversion efficiency of the non-linear waveguide as a function of pump wavelength, without any spectral modulation of the thermal source spectrum by the Michelson interferometer. To do this, we measured the number of photons converted as a function of pump wavelength from 1058 nm to 1080 nm, placing a mask in front of either the Michelson's M_1 mirror or the M_2 mirror, depending on the configuration. It is noteworthy that the two curves obtained are almost identical, indicating that the MIR signal amplitudes in the two arms of the Michelson interferometer are well balanced. Subsequently, these two curves were summed to obtain the reference photometry curve, which incorporates all the experimental parameters (PSD of the thermal source, transmission coefficient of the Michelson interferometer for the signal beam, pump laser power as a function of the wavelength, conversion efficiency. . .).

Finally, the number of converted photons was measured by performing the same pump scan, without any shielding in front of the Michelson interferometer mirrors. The experimental

Optics EXPRESS

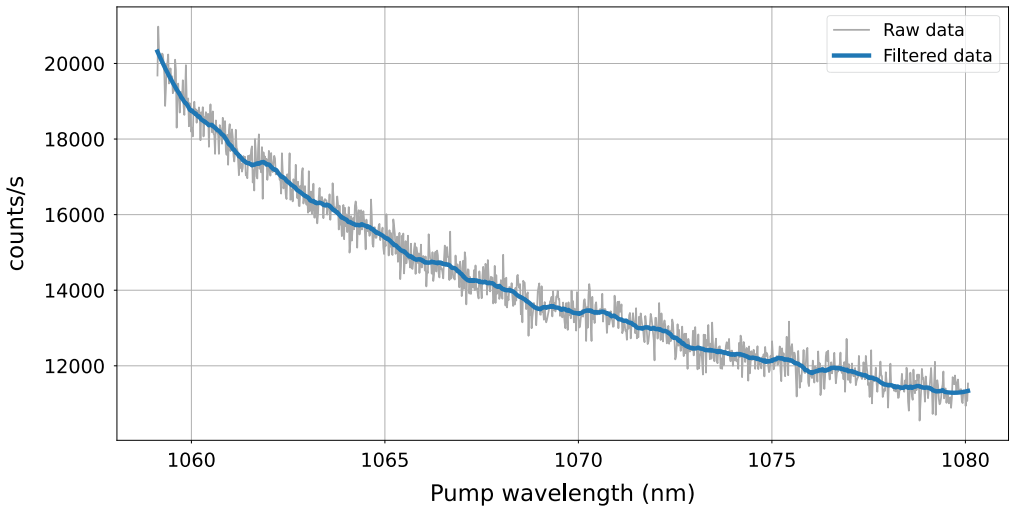

Fig. 3. Background noise of the setup as a function of the pump wavelength. This phenomenon is attributed to the process of spontaneous parametric down conversion. Gray: raw data, blue: filtered data using a Savitzky-Golay filter.

conditions are the exact same as the previous scans, except now the signal beam undergoes spectral modulation.

The resulting curves are displayed in Fig. 4. The background noise that has been recorded previously has been removed from all recordings. As with the measurement of background noise, a decrease in conversion efficiency is observed as the pump wavelength increases during the scan. The reference photometry curve, devoid of spectral modulation, underwent smoothing through the application of a Savitzky-Golay filter. The signal curve obtained when the thermal source is spectrally modulated evidently demonstrates this modulation when the pump wavelength is scanned, that is, when the mid-infrared spectrum of the source is sampled. It is important to note, however, that the modulation amplitude does not reach its maximum potential. This phenomenon is associated with the spectral acceptance width of the non-linear waveguide, as we'll see later in this paper.

In order to reconstruct the spectrum of the spectrally modulated source, it is necessary, for each pump wavelength, to determine the wavelength of the MIR signal corresponding to the quasi-phase-matching of the SFG process. A preliminary approach to determining this correspondence is to use numerical simulations. It is unfortunate that the quasi-phase-matching conditions are highly dependent on experimental parameters, in particular the physical characteristics of the non-linear waveguide, such as its transverse dimensional variations. We have opted for an experimental determination, in which we measure the spectral acceptance (spectrum of the converted signal around 820 nm) for different pump wavelengths. To this end, a diffraction grating spectrometer was integrated at the output of the experimental setup, between the filter stage and the photon counter. The incident beam is collimated at the collecting fiber output in the direction of the diffraction grating, and the light diffracted in the first order is injected into a single-mode optical fiber, which is connected to the filtering stage and finally the photon counter. The spectrometer's resolution is measured to be 0.3 nm, with the primary limitation stemming from the core diameter of the collecting fiber. Note that spectral acceptances need only be measured once to characterize the response of the non-linear waveguide. Then, in normal operation, the non-linear spectrometer no longer requires a diffracting grating spectrometer.

Optics EXPRESS

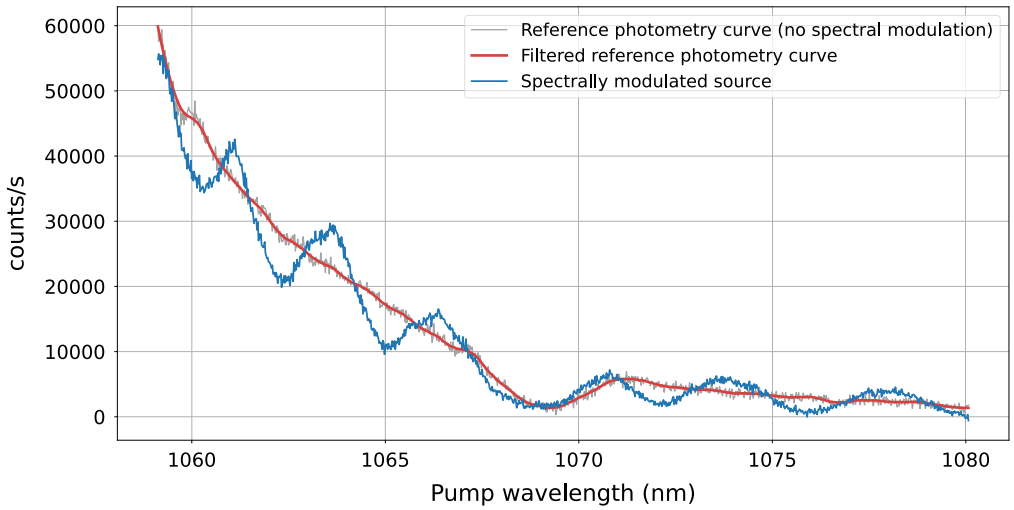

Fig. 4. Number of upconverted photons per second as a function of the pump wavelength. The red curve represents the filtered reference photometry curve, which is the measured upconverted signal from the thermal source when its spectrum is not spectrally modulated by the Michelson interferometer. The blue curve represents the signal curve when the spectral modulation is applied. Background noise, primarily attributed to SPDC generated exclusively by the pump laser, has been subtracted from both recordings.

The measurement of NIR spectral acceptances was conducted for pump wavelengths ranging from 1058 nm to 1080 nm, every 2 nm. Some spectral acceptances are plotted in Fig. 5.

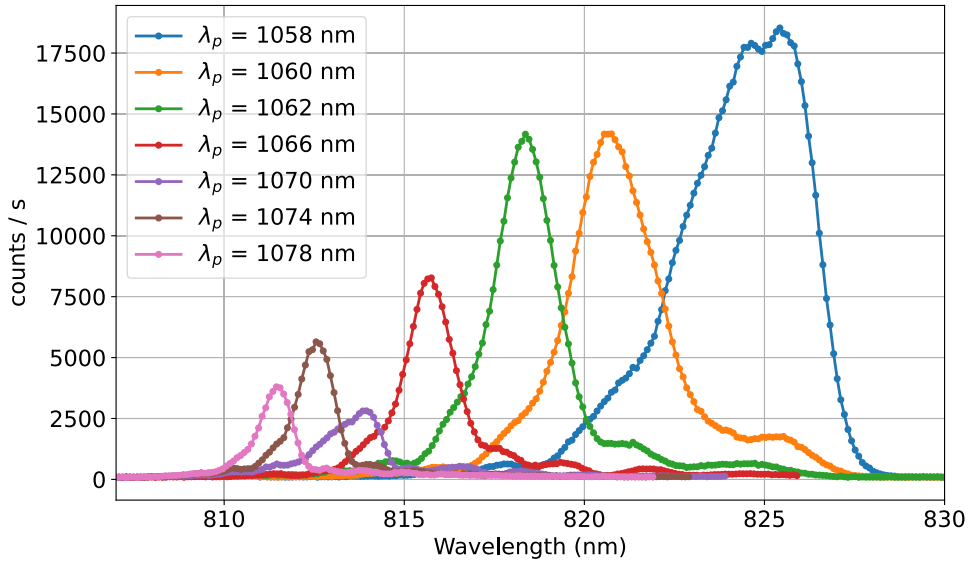

Fig. 5. Measured spectral acceptance curves of the non-linear waveguide for different pump wavelengths

It is observed that the spectral acceptance curves exhibit a general shape that is compatible with the cardinal-square sine model as predicted by the theory. In particular, we note that:

Optics EXPRESS

- The central wavelength of each spectral acceptance decreases as the pump wavelength increases. This may seem counter-intuitive; however, it is associated with the quasi-phase-matching condition of the non-linear process, which depends on the relative evolution of the effective refractive indices of the three interacting waves.
- The discrepancies between the measured spectral acceptance curves and the curves given by theory can be explained, on the one hand, by fluctuations in the transverse dimensions of the waveguide along its length and, on the other hand, by a possible weak coupling of higher-order modes for the pump. This would then give rise to phase matches that are slightly shifted spectrally, although less effective due to poor spatial overlap between the interacting modes.
- The width of spectral acceptances decreases as the pump wavelength increases. This behavior is consistent with the numerical simulations depicted in Fig. 1. However, the experimentally measured variation is considerably greater than the theoretical model's prediction.
- The amplitude of the spectral acceptances undergoes substantial modification in accordance with the pump wavelength. In particular, the integral of each of these acceptances for each pump wavelength is fully compatible with the efficiency curves obtained in Fig. 4, with in particular a maximum conversion efficiency at 1058 nm, and a low conversion efficiency around 1070 nm.

For these last two points, further study is needed to understand the origin of this spectral acceptance behavior.

For each pump wavelength, we determined the central wavelength of spectral acceptance in the NIR. The energy conservation relation of the non-linear process (see Eq. (1)) was used to plot the evolution of the central wavelength of the MIR sample, that is the MIR wavelength associated with maximum conversion efficiency (quasi-phase-matching) as a function of pump wavelength in Fig. 6. It can be seen that the experimental results do not match the simulation shown in Fig. 1. For a given pump wavelength, the average wavelength of the corresponding MIR spectral sample is about 100 nm higher experimentally than predicted by the simulation. We attribute this discrepancy to poor knowledge of the real transverse dimensions of the non-linear waveguide.

The normalized PSD of the thermal source was then obtained by dividing the modulated curve by the reference photometry curve (see Fig. 4), so as to isolate only the thermal source spectrum's contribution to the measured signal. Figure 7 plots this ratio as a function of the frequency of the MIR signal (lower horizontal axis) and as a function of the corresponding MIR wavelength (upper horizontal axis). We used the fitting curve in Fig. 6 to replace a pump wavelength scale with the corresponding MIR wavelength scale.

We clearly observe a periodic modulation in the reconstructed PSD of the thermal source, consistent with Eq. (4). To evaluate the modulation period, we performed a numerical fit of the experimental data as a function of signal frequency, using a sinusoidal function model. The amplitude of this model is modulated by a fourth-order polynomial envelope to take the modulation contrast change into account (this contrast change origin is discussed below). There is very good agreement between the experimental data and the fit curve. The modulation period of the PSD was obtained from the curve fitting parameters, and we find $\Delta\nu_{\mathrm{exp}} = 1.62$ THz. For reference, the expected value was $\Delta\nu = 1.67 \pm 0.15$ THz, a relative deviation of just 3%.

The PSD of the thermal source has little noise at long MIR wavelengths, becoming increasingly noisy as the MIR wavelength decreases. This phenomenon is linked to the fact that the high PSD wavelength part of the source is scanned for short pump wavelengths at the start of the scan, when non-linear conversion efficiency is at its highest. This results in an excellent signal-to-noise ratio. Conversely, as the MIR wavelength decreases, the corresponding pump wavelength increases, and

Optics EXPRESS

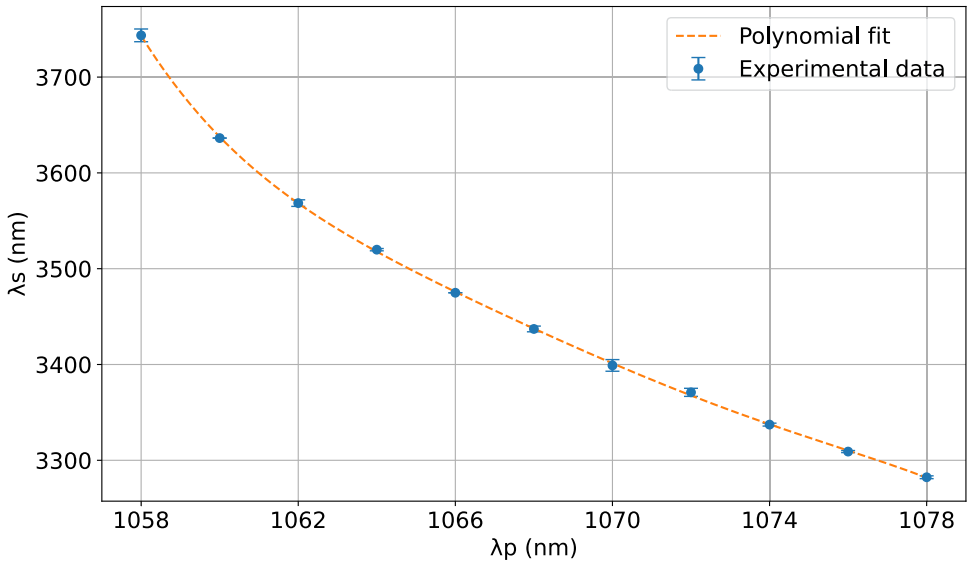

Fig. 6. Center wavelength of the converted MIR spectral sample as a function of the pump wavelength

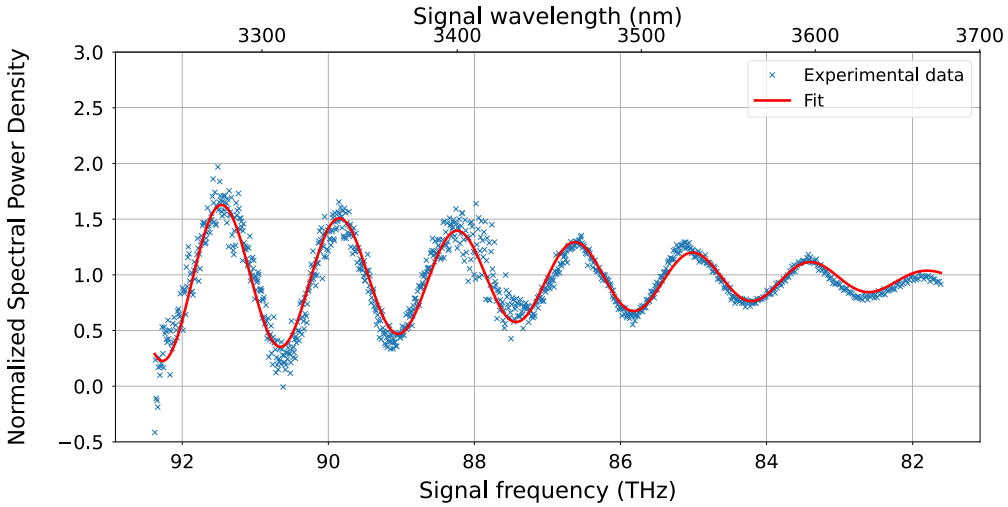

Fig. 7. Reconstructed normalized PSD of the thermal source, indicated in terms of MIR signal frequency (bottom axis) and wavelength (top axis). In blue is the experimental data and in red is the best fit using sinusoidal function with decaying amplitude.

the non-linear conversion efficiency drops, thereby decreasing the signal-to-noise ratio. There is significant noise around the 3.4 µm MIR wavelength, which corresponds to the 1069 nm pump wavelength, where the conversion efficiency is very low (see Fig. 4).

We can also observe a change of modulation contrast in the reconstructed PSD, due to the variation of the spectral acceptance FWHM during the scan. It is much higher at lower pump wavelengths than at higher wavelengths, as seen in Fig. 5. For lower pump wavelengths, the FWHM of the spectral acceptance is greater than the MIR spectral modulation period. As scanning continues, the effect of the change in the intensity of the MIR signal due to modulation

Optics EXPRESS

is mostly averaged out. This is consistent with Eq. (2), which states that the number of converted photons for a given pump wavelength is equal to the overlap integral between the MIR spectrum $B(\nu_s)$ and the spectral acceptance $\eta(\nu_s)$. Conversely, when the pump wavelength is high enough, the FWHM of the spectral acceptance is less than the modulation period, resulting in high modulation contrast in the reconstructed PSD.

The spectral Resolving Power (RP) of the spectrometer in the NIR can be written as follows:

$$\mathrm{R_{NIR}} = \frac{\lambda_c}{\Delta\lambda_c}$$

where λ_c corresponds to the central converted wavelength of the spectral acceptance, and $\Delta\lambda_c$ is the FWHM of this spectral acceptance (see Fig. 5). During upconversion, the spectral sample in the MIR of width $\Delta\nu_s$ is simply transposed into the NIR domain so that $\Delta\nu_c = \Delta\nu_s$ (see section 2). Taking this condition into account, the RP of the non-linear spectrometer in the MIR is written as:

$$\mathrm{R_{MIR}} = \frac{\lambda_c^2}{\lambda_s \Delta\lambda_c}$$

The RP of the non-linear spectrometer in the MIR therefore depends directly on the spectral acceptance width of the non-linear waveguide. In our case, the RP in the MIR ranges from 173 at $\lambda_s = 3.28$ µm to 45 at $\lambda_s = 3.75$ µm. Generally speaking, spectral acceptance widths in the MIR are about twice as large experimentally as those obtained by simulation (Fig. 1). This discrepancy is probably due to fluctuations in the transverse dimensions of the non-linear waveguide over the 2 cm of propagation.

5. Conclusion

This study introduces a novel technique for MIR spectroscopy that enables room-temperature detection by taking advantage of the non-linear process of upconversion. This approach addresses key limitations of conventional methods, such as the need for cryogenic coolers and susceptibility to mechanical vibrations in standard FTIR spectroscopy, or the large footprint and high power requirements of some existing upconversion techniques. The core of our experiment is a 2 cm-long PPLN ridge waveguide, which efficiently converts MIR radiation (specifically between 3 and 4 µm) to NIR around 820 nm. The MIR source spectrum is scanned using a tunable pump laser so the non-linear spectrometer does not need any diffractive element. The upconversion allows for detection with Si-APD photon-counter, which offers a significantly better signal-to-noise ratio compared to MIR detectors at room temperature.

The reliability of the technique presented in this paper is experimentally validated by introducing a Michelson interferometer between a thermal source and the non-linear spectrometer to modulate the spectrum of the source. By continuously scanning the pump laser wavelength, the modulation period was retrieved after upconversion. The experimentally obtained modulation period of 1.62 THz showed a relative error of just 3% compared to the expected 1.67(15) THz, confirming the method's accuracy in reconstructing the MIR source's PSD. The resolving power of the non-linear spectrometer in the MIR ranges from 173 at $\lambda_s = 3.28$ µm to 45 at $\lambda_s = 3.75$ µm

However, there are a few things that have to be taken care of.

- Firstly, we have shown that the spectral acceptance width changes with pump wavelength. Each waveguide must therefore be characterized experimentally to determine its specific Spectral Conversion Matrix. This can be done by measuring the spectral acceptances for a limited number of pump wavelengths, which gives us a sparse matrix, and then filling in the missing data using interpolation techniques. The original MIR spectrum can be recovered using various techniques such as direct matrix inversion, Bayesian deconvolution, or deep learning algorithms. We will study this deconvolution process and its sensitivity to noise in a later work.

Optics EXPRESS

- Secondly, we used a Savitzky-Golay filter to remove high frequency fluctuations from SPDC background noise and reference photometry curve. However, we can't use such a filter for the "science" curve, as spectral information can get lost because of oversampling of the filter. Therefore, noise can make it difficult to recover sharp spectral detail in the MIR spectrum.

In conclusion, we have successfully demonstrated a robust, room-temperature MIR spectroscopy technique based on SFG in a PPLN ridge waveguide, enabling the transfer of MIR spectral information into the NIR domain for detection by highly sensitive silicon detectors. The converted spectral band in this study was between 3.3 µm and 3.7 µm, but it is possible to work on a much wider range as long as the signal to be converted remains within the transparency window of lithium niobate (up to 5 µm) and the non-linear waveguide is designed to achieve phase matching over the target range (by wisely choosing the poling period and the transverse dimensions of the waveguide).

This approach also offers a promising pathway for miniaturized and practical MIR spectroscopic tools for diverse applications. While our current demonstration focuses on spectrally modulated thermal source characterization, the technique is particularly promising for greenhouse gas monitoring applications. For methane detection, our approach provides immediate capability by accessing the fundamental absorption band at 3.3 µm, which exhibits two order of magnitude stronger line strength compared to the second overtone band at 1.65 µm used in conventional NIR laser spectroscopy systems. For carbon monoxide (CO) and nitrous oxide (N_2O) detection, while their fundamental absorption bands at 4.5-4.6 µm lie outside our current spectral coverage (3.1-3.7 µm), a clear technical pathway exists for spectral extension. Using the same pump laser (around 1064 nm), specialized PPLN waveguides with tailored poling periods ($\Lambda \approx 19.4$ µm for CO at 4.6 µm, and $\Lambda \approx 19.5$ µm for N_2O at 4.5 µm) can be implemented in a parallel configuration.

Funding. Agence Nationale de la Recherche (ANR-23-PEEL-0004, ANR-21-ESRE-0040, ANR-17-EURE-0002).

Acknowledgment. This work has been financially supported by Thales Alenia Space and CPER : FEDER PILIM Nouvelle Aquitaine 2025-2027. M. Chauvet acknowledges the supports of the French Agence Nationale de la Recherche under projects NanoFiLN (ANR-23-PEEL-0004), EQUIPEX+ SMARTLIGHT platform (ANR-21-ESRE-0040) and EIPHI Graduate School (ANR-17-EURE-0002). This work was also partly supported by the French RENATECH network, MIMENTO technological facility, and the Région Bourgogne Franche-Comté.

Disclosures. The authors declare no conflicts of interest.

Data availability. Data underlying the results presented in this paper are not publicly available at this time but may be obtained from the authors upon reasonable request.

References

1. A. Lux, R. Müller, M. Tulk, *et al.*, "HHT diagnosis by Mid-infrared spectroscopy and artificial neural network analysis," Orphanet J. Rare Dis. **8**(1), 94 (2013). Publisher: Springer Science and Business Media LLC.
2. B. Van Eerdenbrugh and L. S. Taylor, "Application of mid-IR spectroscopy for the characterization of pharmaceutical systems," Int. J. Pharm. **417**(1-2), 3–16 (2011). Publisher: Elsevier BV.
3. A. O. Petric, L. Armus, J. Howell, *et al.*, "Mid-Infrared Spectral Diagnostics of Luminous Infrared Galaxies," The Astrophys. J. **730**(1), 28 (2011). Publisher: American Astronomical Society.
4. L. Flannigan, L. Yoell, and C.-q. Xu, "Mid-wave and long-wave infrared transmitters and detectors for optical satellite communications—a review," J. Opt. **24**(4), 043002 (2022). Publisher: IOP Publishing.
5. D. Popa and F. Udrea, "Towards Integrated Mid-Infrared Gas Sensors," Sensors **19**(9), 2076 (2019). Publisher: MDPI AG.
6. P. F. Bernath, *Spectra of atoms and molecules* (Oxford university press, New York, 2016), 3rd ed.
7. E. D. Becker and T. C. Farrar, "Fourier Transform Spectroscopy: New methods dramatically improve the sensitivity of infrared and nuclear magnetic resonance spectroscopy," Science **178**(4059), 361–368 (1972). Publisher: American Association for the Advancement of Science (AAAS).
8. F. Adler, P. Maslowski, A. Foltynowicz, *et al.*, "Mid-infrared Fourier transform spectroscopy with a broadband frequency comb," Opt. Express **18**(21), 21861 (2010). Publisher: Optica Publishing Group.
9. A. Rogalski, *Infrared detectors* (CRC Press, Taylor & Francis, Boca Raton, 2011), 2 edition ed.

Optics EXPRESS

10. W. H. Louisell, A. Yariv, and A. E. Siegman, "Quantum Fluctuations and Noise in Parametric Processes. I," Phys. Rev. **124**(6), 1646–1654 (1961).
11. K. E. Jahromi, Q. Pan, L. Høgstedt, *et al.*, "Mid-infrared supercontinuum-based upconversion detection for trace gas sensing," Opt. Express **27**(17), 24469 (2019). Publisher: Optica Publishing Group.
12. J. S. Dam, P. Tidemand-Lichtenberg, and C. Pedersen, "Room-temperature mid-infrared single-photon spectral imaging," Nat. Photonics **6**(11), 788–793 (2012).
13. R. W. Boyd, *Nonlinear Optics* (Acad. Press, 2003).
14. T. Kashak, L. Flannigan, A. Atwi, *et al.*, "Compact intracavity mid-infrared upconversion detector – a systematic study," Opt. Continuum **3**(9), 1660 (2024). Publisher: Optica Publishing Group.
15. S. M. M. Friis and L. Høgstedt, "Upconversion-based mid-infrared spectrometer using intra-cavity $LiNbO_3$ crystals with chirped poling structure," Opt. Lett. **44**(17), 4231 (2019). Publisher: Optica Publishing Group.
16. A. Barh, M. Tawfieq, B. Sumpf, *et al.*, "Upconversion spectral response tailoring using fanout QPM structures," Opt. Lett. **44**(11), 2847 (2019). Publisher: Optica Publishing Group.
17. P. Tidemand-Lichtenberg, M. Aagaard, A. S. Ashik, *et al.*, "Tunable infrared upconversion module for the 1.9 to 5.5 μm range," Opt. Lett. **47**(23), 6189 (2022). Publisher: Optica Publishing Group.
18. A. Barh, C. Pedersen, and P. Tidemand-Lichtenberg, "Ultra-broadband mid-wave-IR upconversion detection," Opt. Lett. **42**(8), 1504 (2017). Publisher: Optica Publishing Group.
19. L. Lehmann, L. Grossard, L. Delage, *et al.*, "Single photon MIR upconversion detector at room temperature with a PPLN ridge waveguide," Opt. Express **27**(14), 19233 (2019).
20. R. Penrose, "A generalized inverse for matrices," Math. Proc. Cambridge Philos. Soc. **51**(3), 406–413 (1955). Publisher: Cambridge University Press (CUP).
21. J. S. Pelc, C. Langrock, Q. Zhang, *et al.*, "Influence of domain disorder on parametric noise in quasi-phase-matched quantum frequency converters," Opt. Lett. **35**(16), 2804 (2010). Publisher: Optica Publishing Group.
22. M. A. Albota and F. N. C. Wong, "Efficient single-photon counting at 1.55 μm by means of frequency upconversion," Opt. Lett. **29**(13), 1449 (2004). Publisher: Optica Publishing Group.
23. J. Li, H. Deng, P. Li, *et al.*, "Real-time infrared gas detection based on an adaptive Savitzky–Golay algorithm," Appl. Phys. B **120**(2), 207–216 (2015).